International Information and Engineering Technology Association
Advancing the World of Information and Engineering

Journal Européen des Systèmes Automatisés
Vol. 59, No. 7, July, 2026, pp. 1945-1957
Journal homepage: http://iieta.org/journals/jesa

High-Fidelity Modelling and Multi-Objective Hybrid GWO-PSO Tuned PI Controllers: Applied to Pitch Control for Large Wind Turbines in Region III Operation

Dari Hadjer, Mehennaoui Lamine, Soudani M. Lamine, Youcef Zennir*

Automatic Laboratory of Skikda, Skikda University, Skikda 21000, Algeria

Corresponding Author Email: y.zennir@univ-skikda.dz

https://doi.org/10.18280/jesa.590711

Received: 14 May 2026
Revised: 13 July 2026
Accepted: 20 July 2026
Available online: 31 July 2026

Keywords:
large wind turbine, high-fidelity modeling, pitch angle control, meta-heuristic optimization, hybrid Grey Wolf-Particle Swarm Optimization

ABSTRACT

The rapid evolution of utility-scale wind turbines with rated capacities exceeding 5 MW has increased the complexity of pitch control under above-rated wind conditions. Conventional proportional-integral (PI) controllers often exhibit limited performance due to nonlinear aerodynamic behavior, drive-train flexibility, actuator constraints, and turbulent wind disturbances. This paper proposes a hybrid Grey Wolf Optimizer-Particle Swarm Optimization (HGWO-PSO) algorithm for the automatic tuning of a PI pitch controller applied to a high-fidelity nonlinear aero-mechanical wind turbine model. The model incorporates nonlinear aerodynamics, a two-mass rotor–generator drive-train, a constrained pitch actuator, and a smooth Region II-III operating strategy that combines maximum power point tracking below the rated wind speed with pitch-based speed regulation above the rated wind speed. The proposed hybrid algorithm combines the exploration capability of GWO with the exploitation ability of PSO to improve convergence and optimization accuracy. Its performance is compared with PSO, GWO, Differential Evolution (DE), and Genetic Algorithm (GA) using the integral absolute error (IAE), integral time-weighted absolute error (ITAE), overshoot, and cumulative pitch travel as performance indices. Simulation results under turbulent wind conditions demonstrate that the proposed HGWO-PSO controller provides more accurate generator-speed regulation, smoother pitch activity, and improved optimization performance compared with the individual optimization algorithms.

1. INTRODUCTION

Wind power has been recognized as a vital and sustainable strategy to meet the growing global energy demand by providing clean and renewable energy resources [1-5]. The increasing demand for electricity has accelerated the deployment of large-scale wind turbines, which are commonly rated above 5 MW [6]. These large wind turbines operate under highly variable and stochastic wind conditions, where turbulence, gusts, and wind ramps create complex interactions between the aerodynamic subsystem, drive-train flexibility, and the control system [7]. Advanced control strategies are required to ensure reliable operation, efficient energy capture, and satisfactory dynamic performance under varying wind conditions [8, 9]. The objectives of the control strategy depend on the operating region of the wind turbine [10, 11]. When the wind speed exceeds the rated value (Region III), the control objective shifts from maximum power extraction to maintaining the generator speed close to its rated value while limiting excessive aerodynamic loading on the drive-train. In this region, the coordinated adjustment of all blade pitch angles is the primary mechanism used to regulate the aerodynamic torque and protect the drive-train and other load-carrying components [6, 7, 12]. The proportional-integral (PI) controller is widely used because of its simple structure and satisfactory performance around an operating point [13, 14]. However, nonlinear aerodynamic characteristics, flexible rotor–shaft–generator dynamics, pitch actuator saturation and rate constraints create a strongly nonlinear and coupled control environment. Turbulent wind conditions significantly affect controller performance, making conventional PI tuning methods less effective and often requiring manual adjustment, which may lead to suboptimal performance [15]. To improve the automatic tuning of PI or PID controllers for wind energy conversion systems (WECSs), several meta-heuristic optimization algorithms, including PSO, Grey Wolf Optimizer (GWO), Genetic Algorithm (GA), and Differential Evolution (DE), have been proposed [16-19]. These algorithms have demonstrated satisfactory performance in controller optimization, improving dynamic response and control accuracy in WECSs [20, 21]. However, single meta-heuristic algorithms often exhibit an imbalance between global exploration and local exploitation, which may lead to premature convergence or reduced search efficiency when solving complex nonlinear constrained optimization problems [14, 15]. To address these limitations, hybrid optimization strategies combining the strong exploration capability of GWO with the efficient local exploitation of PSO have recently attracted considerable attention [22, 23]. Although hybrid optimization methods have demonstrated promising performance in various engineering optimization problems, their application to PI pitch controller tuning for large-scale wind turbines operating in Region III remains limited. In particular, few studies simultaneously consider nonlinear aerodynamic characteristics, a flexible two-mass drive-train, pitch actuator dynamics, and turbulent wind conditions [14, 15, 24]. This constitutes the primary research gap addressed in the present work. Besides meta-heuristic optimization techniques, model-based control approaches such as Model Predictive Control (MPC) [15, 25] and robust H∞ control [26-28] have been investigated for wind turbine pitch regulation because of their ability to explicitly handle constraints and disturbances. Although these advanced control strategies provide improved dynamic performance, they generally require more accurate mathematical models and involve higher computational complexity. Therefore, optimized PI controllers remain an attractive industrial solution because of their simplicity, robustness, and ease of implementation. Recent studies have also shown that actuator constraints, drive-train flexibility, and turbulent wind disturbances play a significant role in the overall performance of pitch control systems [9]. For instance, Rezaei et al. [7] investigated the influence of wind field characteristics and pitch actuator duty cycles on the reliability and fatigue life of the pitch bearing in the NREL 5 MW wind turbine. Hummel et al. [8] highlighted the trade-off between aggressive blade load reduction and increased pitch actuator effort in output-constrained individual pitch control. These observations indicate that controller assessment should not rely solely on classical tracking performance indices such as the integral absolute error (IAE) or the integral time-weighted absolute error (ITAE), but should also consider actuator-related indicators, including cumulative pitch travel. Motivated by these observations, this paper proposes a hybrid Grey Wolf Optimizer-Particle Swarm Optimization (HGWO-PSO) algorithm for the automatic tuning of a PI pitch controller for the NREL 5 MW wind turbine. The controller is evaluated using a high-fidelity control-oriented nonlinear aero-mechanical wind turbine model incorporating nonlinear aerodynamics, a flexible two-mass drive-train, a constrained pitch actuator, and a smooth Region II-III operating transition. The proposed HGWO-PSO algorithm is compared with PSO, GWO, GA, and DE using a multi-objective performance index based on the IAE, ITAE, overshoot, and cumulative pitch travel under turbulent wind conditions. The remainder of this paper is organized as follows. Section 2 describes the nonlinear wind turbine model. Section 3 presents the PI pitch control strategy and the optimization problem formulation. Section 4 introduces the investigated meta-heuristic optimization algorithms and the proposed HGWO-PSO approach. Section 5 discusses simulation results. Finally, Section 6 presents the conclusions.

2. WIND TURBINE MODEL

The studied wind turbine model is a NREL-5MW variable-speed and variable-pitch horizontal axis wind turbine. Figure 1 outlines the overall block diagram of the proposed wind turbine control system. The mathematical modeling of the wind turbine is provided, with the major components of a typical wind turbine including the aerodynamic system, the drive-train, the generator, the pitch angle actuator, and the control unit, which are described in the following subsections.

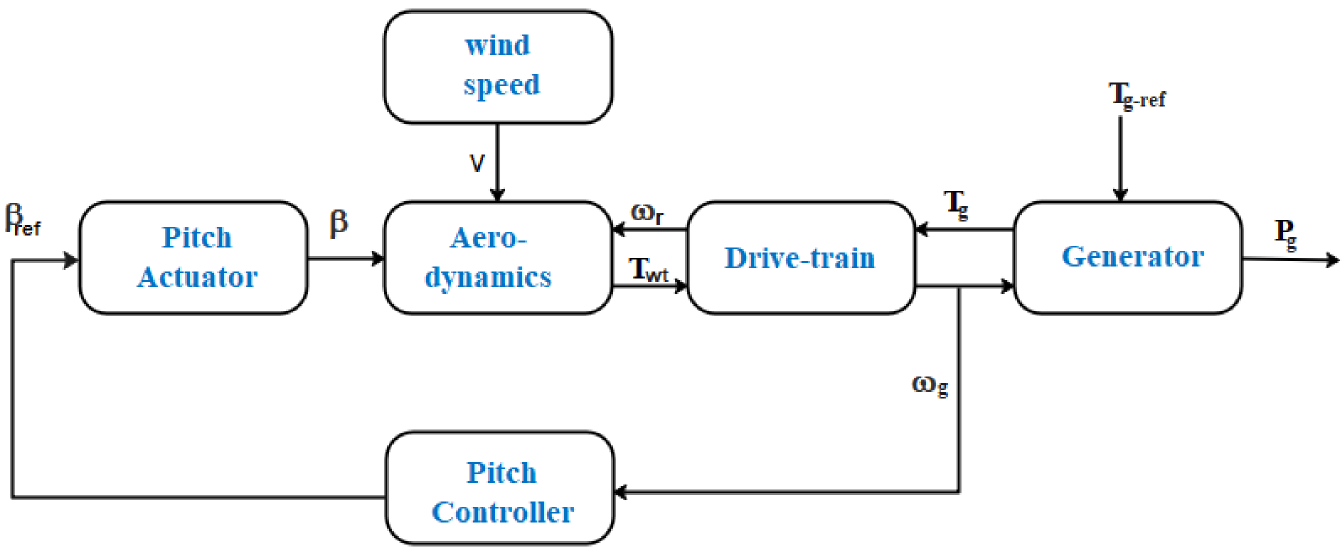

Figure 1. Wind turbine overall block diagram

2.1 Aerodynamics model

The aerodynamic torque of the wind turbine T_{wt} is given by the following expression [29]:

$$T_{wt} = 0.5\rho\pi R^3 C_q(\lambda,\beta)V^2 \tag{1}$$

where, $C_q(\lambda, \beta)$ is defined as:

$$C_q(\lambda,\beta) = \frac{1}{\lambda}C_p(\lambda,\beta) \tag{2}$$

where, ρ is the air density, R is the blade length, and V is the wind speed. C_q is the power coefficient, which is defined by:

$$\begin{aligned} C_p(\lambda,\beta) &= c_1\left(c_2\left(\frac{1}{\lambda+0.08\beta}-\frac{0.035}{\beta^3+1}\right)-c_3\beta-c_4\right) \\ &\times\exp\left(-c_5\left(\frac{1}{\lambda+0.08\beta}-\frac{0.035}{\beta^3+1}\right)\right)+C_6\lambda \end{aligned} \tag{3}$$

where, β is the pitch angle, and λ is the tip ratio of the wind turbine, which expresses the ratio between the peripheral blade speed and the wind speed, and is computed as [30, 31].

$$\lambda = \frac{\omega_r R}{V} \tag{4}$$

The aerodynamic coefficients c_i are {0.5176, 116, 0.4, -5, -21, 0.0068} [32, 33]. Figure 2 gives the variation of C_p as a function of λ and β.

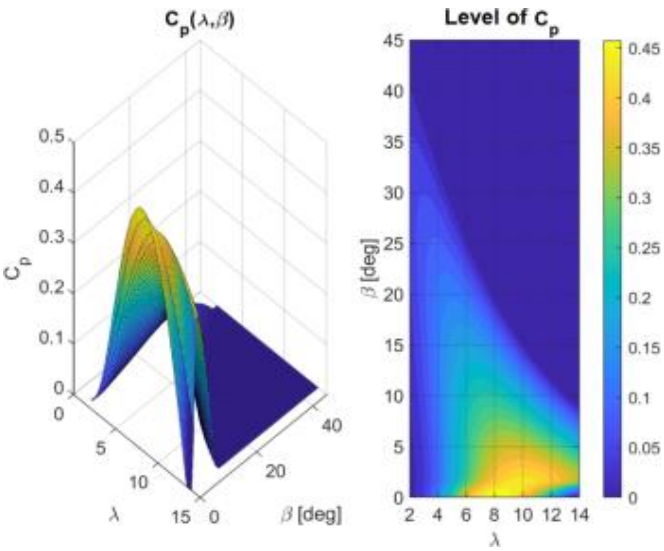

Figure 2. Power coefficient variation

2.2 Two-mass drive-train model

The power is transferred from the rotor shaft to the generator shaft by a component called the drive-train system. Typically, there are three different models (one-mass, two-mass, and three-mass models) [34]. We used the two-mass model as shown in Figure 3 to model this system.

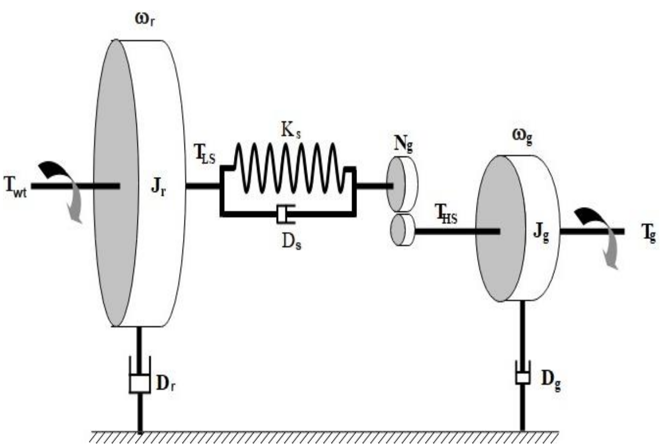

Figure 3. Wind turbine drive-train dynamic model

This model helps to manage the load distribution and smooth the power transmitted to the generator, while allowing the development of advanced control systems to optimize energy efficiency and prevent failures through anomaly detection. The rotor inertia J_r is modeled by the following equation [35-37]:

$$J_g\ \omega_g = T_{\omega t} - T_{LS} - D_r\ \omega_r \tag{5}$$

The low-speed torque T_{LS} is modeled by:

$$T_{LS} = K_s\left(\psi_r - \psi_{LS}\right) + D_s\left(\omega_r - \omega_{LS}\right) \tag{6}$$

The generator inertia J_g is modeled by:

$$J_g\ \omega_g = T_{HS} - T_g - D_g\ \omega_g \tag{7}$$

In the case of an ideal gearbox, the relationship between the torque and the speed of this shaft is given by:

$$\eta_g = \frac{T_{LS}}{T_{HS}} = \frac{\omega_g}{\omega_{LS}} = \frac{\psi_g}{\psi_{LS}} \tag{8}$$

By using the relations from Eqs. (5) to (8), the following system is then derived:

$$\begin{bmatrix}\omega_r\\ \omega_g\\ T_{LS}\end{bmatrix} = \begin{pmatrix}a_{11} & a_{12} & a_{13}\\ a_{21} & a_{22} & a_{23}\\ a_{31} & a_{32} & a_{33}\end{pmatrix}\begin{bmatrix}\omega_r\\ \omega_g\\ T_{LS}\end{bmatrix} + \begin{bmatrix}b_{11}\\ b_{21}\\ b_{31}\end{bmatrix} T_{\omega t} + \begin{bmatrix}b_{12}\\ b_{22}\\ b_{32}\end{bmatrix} T_g \tag{9}$$

where,

$a_{11} = -\frac{D_r}{J_r}$, $a_{12} = 0$, $a_{13} = -\frac{1}{J_r}$, $a_{21} = 0$,
$a_{22} = -\frac{D_g}{J_g}$, $a_{23} = \frac{1}{\eta_g J_g}$, $a_{31} = K_s - \frac{D_s D_r}{J_r}$,
$a_{32} = \frac{1}{\eta_g}\left(\frac{D_s D_g}{J_g} - K_s\right)$, $a_{33} = \frac{-D_s\left(J_r + \eta_g^2 J_g\right)}{\eta_g^2 J_r J_g}$,
$b_{11} = \frac{1}{J_r}$, $b_{21} = 0$, $b_{31} = \frac{D_s}{J_r}$,
$b_{32} = \frac{D_s}{\eta_g J_g}$, $b_{22} = -\frac{1}{J_g}$, $b_{12} = 0$.

where, D_s is the low-speed shaft stiffness, D_g is the generator external damping, K_S is the low-speed shaft damping, D_r is the rotor external damping, and η_g is the gearbox ratio. In addition, T_{HS} is the high-speed shaft torque; T_{LS} is the low-speed shaft torque. ψ_g, ψ_{LS} and ψ_r are generator side angular deviation, gearbox side angular deviation and rotor side angular deviation respectively. With ω_g is the generator speed, ω_{LS} is the low-speed shaft speed, and ω_r is the rotor speed.

2.3 Generator model

The generator model we consider is a first-order model as follows [38, 39]:

$$T_g = \frac{1}{\tau_g}\left(T_{g-ref} - T_g\right) \tag{10}$$

where, τ_g is the time constant of the generator.

The generator power P_g captured can be expressed as:

$$P_g = T_g \omega_g \tag{11}$$

The pitch actuator rotates each blade of a wind turbine around its own longitudinal axis. The actuator is modeled as a first-order low-pass filter, which is given by Eq. (12). Figure 4 describes the structure of the pitch angle control system [38-42].

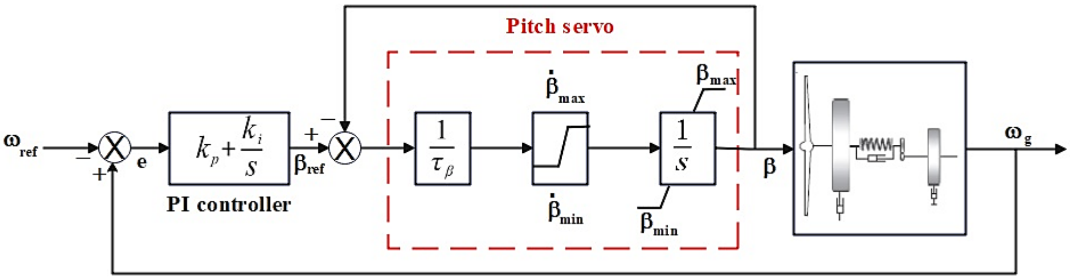

Figure 4. Structure of the pitch angle control system

$$\beta = sat_{[-\beta_{max},\beta_{max}]}\left(\frac{-\beta + \beta_{cmd}}{\tau_\beta}\right) \Leftrightarrow$$
$$\frac{\beta}{\beta_{ref}} = \frac{1}{\tau_\beta s + 1} \qquad (12)$$
$$\beta \in [\beta_{\min}, \beta_{\max}]$$

where, τ_β is the time constant of the pitch actuator. β_{ref} is the actuator's reference angle, which is adjusted by the pitch controller, and β is the current angle of the blades.

2.4 Control unit

The operation of a horizontal axis wind turbine is divided into four regions [43-45]. These regions are divided by the limiting wind speeds, as shown in Figure 5.

Once the wind speed exceeds the cut-in wind speed (V_{cut-in}), the control unit switches to the second region (Region II), which is called the partial load region, where the torque control comes into operation. In this region, the aim is to maximize the power coefficient C_p by maintaining the pitch angle at 0° and adjusting the generator torque.

The latter reaches its maximum value when the pitch angle β and the speed ratio λ are optimal. Mathematically, we have:

$$C_{p-\max} = C\left|\begin{matrix}\beta = \beta_{opt} \\ \lambda = \lambda_{opt}\end{matrix}\right. \qquad (13)$$

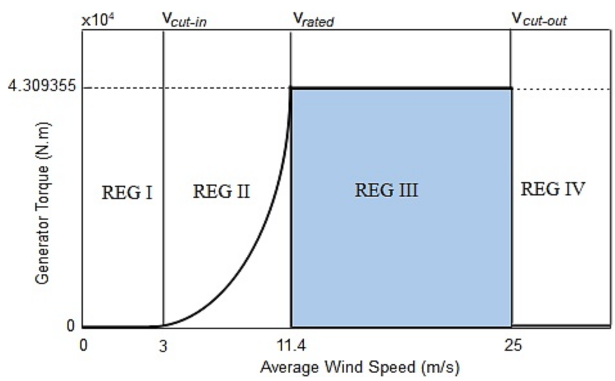

Figure 5. Wind turbine operating regions

For the 5 MW model, the optimal values are $\beta = 0^\circ$ and $\lambda = 7.55$. At these values, we have $C_{p-max} = 0.482$. In this region we describe the control law for T_{g-ref} by the equation below (Eq. (14)) [20, 37]:

$$T_{g-ref} = K_{opt}\omega_g^2 \qquad (14)$$

where, K_{opt} is obtained from the following equation [38]:

$$K_{opt} = \frac{1}{2\eta_g^3\lambda_{opt}^3}\rho\pi R^5 C_{p-\max} \qquad (15)$$

When the wind speed is higher than the rated speed V_{reted} and lower than the cut-out speed $V_{cut-out}$, the wind turbine operates in region three (Region III), which is called the full-load region. The main control objective in this region is to maintain the generator power P_g around its rated value $P_{g-rated}$. That is, the wind turbine operates at its maximum rated power, and produces energy at its maximum capacity. To achieve this, the control law for T_{g-ref} is given by [36, 41].

$$T_{g-ref} = \frac{P_{g-rated}}{\omega_g} \qquad (16)$$

According to Eqs. (14)-(16) if ω_g be kept around the rated generator speed ω_{ref}, then P_g remains around $P_{g-rated}$. So, in order to keep this goal, the control unit is used to tune the pitch angle.

The generator torque blends smoothly from (Eq. (14)) (Maximum Power Point Tracking (MPPT)) to $T_g = P_{rated}/\omega_g$ $T_g = K_{opt}\omega_g^2$ (Eq. (16)) (rated), using:

$$\sigma(\omega_g) = \frac{1}{1 + \exp\left(-(\omega_g - \omega_{ref})/k\right)} \qquad (17)$$

$$T_g(\omega_g) = (1-\sigma)K_{opt}\omega_g^2 + \sigma\frac{P_{g-rated}}{\max(\omega_g, \omega_{\min})} \qquad (18)$$

We show $\sigma(t)$ alongside ω_g to interpret region three operation (Region III). In the last region (Region IV), when the speeds are above $V_{cut-out}$, the control unit shuts off the wind turbine to protect it from mechanical stresses and high fatigue, which is accomplished by setting the pitch angle to 90°.

3. PITCH CONTROL STRATEGY

In region three (Region III) operations, where wind speeds exceed the rated value, the primary control objective is to regulate generator speed ω_g close to its rated reference ω_{ref}. This is achieved by adjusting the pitch angle β through a feedback controller that modifies the aerodynamic torque T_{wt}. The control law is defined as [13, 20, 37]:

$$\beta(t) = K_p e(t) + K_i\int_0^t e(\tau)d\tau + \beta_0 \qquad (19)$$

With

$$e(t) = \omega_g(t) - \omega_{ref} \tag{20}$$

where, β is the commanded blade pitch angle [deg]; β_0 is the minimum pitch bias (typically 3°); $e(t)$ is the generator speed error, and K_p and K_i, are the proportional and integral gains, respectively. The controller parameters (K_p and K_i) are adjusted by the use of meta-heuristic algorithms such as (PSO, GWO, GA, DE) and the proposed hybrid algorithm (HGWO-PSO) [16-19].

The PI controller gains are determined by minimizing a weighted composite objective function that simultaneously considers tracking accuracy, transient response, and actuator effort given by:

$$J = w_1 IAE + w_2 ITAE + w_3 OS + w_4 E \tag{21}$$

where,

$IAE = \int_0^T |e(t)|\, dt$: is the IAE.

$ITAE = \int_0^T t|e(t)|\, dt$: is the ITAE.

$OS = max\left(0, \omega_g^{max_{ref}}()\right)$: is the overshoot.

$E = \int_0^T |\beta(t)|\, dt$: is the cumulative pitch effort.

Since the performance indices have different physical units and numerical magnitudes, each criterion was first normalized using the corresponding value obtained from the manually tuned PI controller. The weighting coefficients were selected as $w_1 = 0.35$, $w_2 = 0.35$, $w_3 = 0.20$, and $w_4 = 0.10$, giving higher priority to the tracking performance (IAE and ITAE) while still accounting for overshoot and pitch control effort.

The weights satisfy the sum of weights is equal to 1, resulting in a balanced weighted composite objective function. The HGWO-PSO algorithm minimizes the weighted composite objective function and returns a single optimal pair of PI controller gains satisfying the actuator and stability constraints. The optimization seeks:

$$\min_{K_p, K_i} J\left(K_p K_i\right) \tag{22}$$

The controller gains are optimized within the search ranges $K_P \in [0.5,\ 4]$ and $K_i \in [0.1,\ 0.5]$. Subject to actuator and stability constraints:

$$\beta_{\min} \le \beta_{cmd} \le \beta_{\max} \tag{23}$$

$$|\beta| \le \beta_{max} \tag{24}$$

The blade pitch angle is constrained to 3º ≤ β ≤ 45º, while the pitch rate is limited to ∣ β ∣ ≤ 8º/s. To prevent integrator windup during actuator saturation, a back-calculation anti-windup scheme is implemented. The integral-state dynamics are modified according to [46, 47]:

$$\dot{x} = e - K_{aw}\left(\beta_{cmd,sat} - \beta_{cmd}\right) \tag{25}$$

where, $K_{aw} = 3$ is the anti-windup gain, β_{cmd} is the unconstrained controller output, and $\beta_{cmd,sat}$ is the saturated pitch command. This mechanism rapidly removes excessive integral accumulation whenever actuator saturation occurs, thereby improving transient recovery and closed-loop stability.

4. PROPORTIONAL-INTEGRAL CONTROLLER TUNING WITH META-HEURISTIC ALGORITHMS

Meta-heuristic algorithms are optimization techniques based on general search strategies used to solve complex problems independently of their type. They aim to find optimal or near-optimal solutions through efficient exploration of the search space with reasonable computational cost. These methods are particularly effective for nonlinear and large-scale optimization problems where conventional approaches may be inadequate.

The PSO algorithm is inspired by the social behavior of bird flocks. Each particle represents a candidate solution (K_p, K_i) and adjusts its position based on individual and collective best solutions [30, 48].

The principle of the GWO algorithm is based on the leadership hierarchy and hunting behavior of grey wolves. The best three solutions α, β, and δ guide the search, and the position of each candidate is updated as follows [48, 49]:

$$D_\alpha = \left|C_1 X_\alpha - X\right|, X_1 = X_\alpha - A_1 D_\alpha \tag{26}$$

$$D_\delta = \left|C_2 X_\delta - X\right|, X_2 = X_\delta - A_2 D_\delta \tag{27}$$

$$D_\gamma = \left|C_3 X_\gamma - X\right|, X_3 = X_\gamma - A_3 D_\gamma \tag{28}$$

$$X^{t+1} = \frac{X_1 + X_2 + X_3}{3} \tag{29}$$

where, $A_j = 2ar_j - a$, $C_j = 2r_j$, with a decreases linearly from 2 to 0 over iterations, and $r_j \in [0,1]$ are random numbers. The principal of DE algorithm evolves a population by mutation, crossover, and selection operations. A mutant vector is generated as [30, 49]:

$$V = X_r + F\left(X_s - X_t\right) \tag{30}$$

where, F is the mutation factor. Crossover with a target vector produces a trial solution, which replaces the original if it has a lower cost. GA algorithm mimics biological evolution using selection, crossover, and mutation. Candidate solutions are encoded as chromosomes, and fitter individuals are more likely to reproduce. GA is effective in global exploration but may converge slowly near the optimum [49].

To slow exploitation in GWO, a hybrid GWO-PSO (HGWO-PSO) approach is proposed (Figure 6). This method combines the strong global exploration ability of GWO with the efficient local exploitation of PSO under a unified optimization framework. The HGWO-PSO algorithm inherits the global search ability of GWO during early exploration and the rapid convergence of PSO during final exploitation. This hybrid strategy improves the convergence speed and solution quality when solving the non-convex optimization problem. It reduces the risk of premature convergence and provides a better trade-off between tracking performance and cumulative pitch travel. The overall optimization procedure is illustrated in the flowchart shown in Figure 6. Figure 6 presents the complete implementation of the proposed HGWO-PSO algorithm. The optimization starts by initializing the population of candidate PI gains and evaluating the objective function.

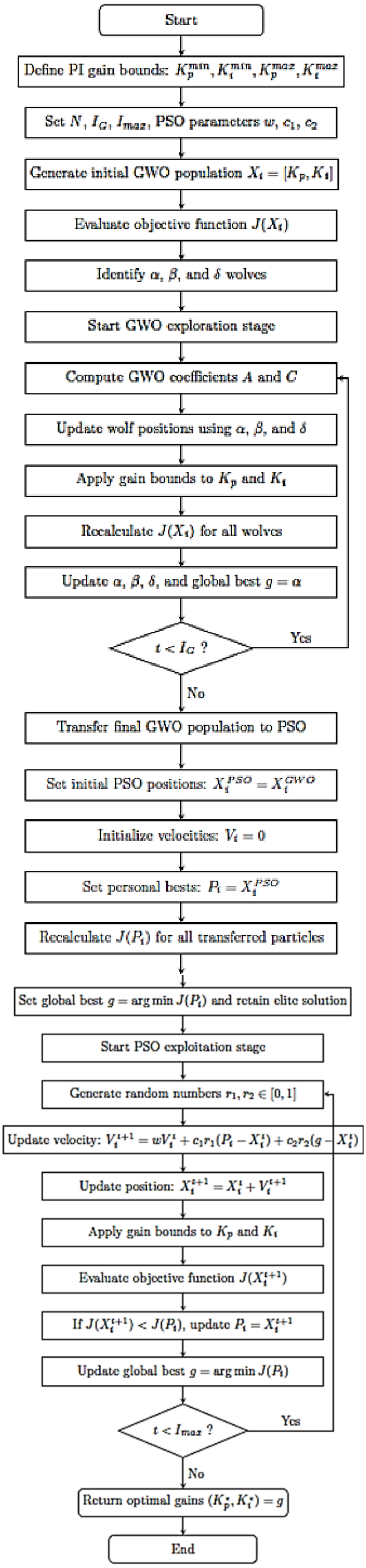

Figure 6. Flowchart of hybrid Grey Wolf Optimizer-Particle Swarm Optimization (HGWO-PSO) algorithm

During the first stage, GWO performs global exploration by updating the positions of the wolves according to the three best solutions (α, β, and δ). At the end of the GWO phase, the final population is directly transferred to the PSO stage. The transferred solutions are used as the initial particle positions, particle velocities are initialized to zero, the objective function is re-evaluated to initialize the personal-best positions, and the alpha wolf is retained as the initial global-best solution. The PSO stage then performs local exploitation through velocity and position updates until the maximum number of iterations is reached. Finally, the optimal PI controller gains are returned.

5. RESULTS AND DISCUSSION

All optimization algorithms (PSO, GWO, GA, DE, and the proposed HGWO-PSO) were evaluated under identical operating conditions using the nonlinear 5 MW NREL reference wind turbine operating in Region II-III. The complete aero-mechanical model described in Section 2 was implemented in MATLAB. The simulation parameters and optimization settings are summarized in Tables 1 [37] and 2. For a fair comparison, all algorithms used the same objective function (Eq. (22)), search space, population size, and maximum number of iterations.

Table 1. Plant parameters used for Region II-III pitch control studies (NREL 5MW)

Parameter	Symbol / Value
Air density	$\rho = 1.225$ Kg.m^{-3}
Rotor radius	R = 63 m
Gear ratio	$N_g = 97$
Rotor inertia	$J_r = 3.8759227 \times 10^7$ Kg.m^2
Generator inertia	$J_g = 534.1$ Kg.m^2
Shaft stiffness	$K_s = 92214$ Nm.rad^{-1}
Shaft (torsional) damping	$D_s = 660.47$ Nm.s.rad^{-1}
Rated generator speed	$\omega_{ref} = 122.9$ rad. s^{-1}
Rated electrical power	$P_{rated} = 5$ MW
Rated generator torque	$T_{g\text{-}ref} = 43093.55$ N.m
Rated generator torque max	$T_{g,rate\text{-}max} = 15000$ N.m.s^{-1}
Pitch lower/upper limits	$\beta_{min} = 3$, $\beta_{max} = 45$ deg
Pitch rate limit	$d\beta_{max} = 8$ deg.s^{-1}
Wind range (simulation)	$V \in [11.4, 25]$ m.s^{-1}
Sampling grid	$\Delta t = 0.01$, $T_{end} = 300$ s

Table 2. Algorithm parameters for proportional-integral (PI) tuning and shared optimization settings (population = 30; iteration = 100)

Optimizer	Parametres
PSO	$w_{max} = 0.95$, $w_{min} = 0.20$, $c_1 = 1.9$, $c_2 = 1.7$
DE	F = 0.6, CR = 0.9
GWO	Oppositional restart fraction 0.30
GA	BLX-a crossover (α = 0.5), mutation prob. 0, 25, σ = 0.15
HGWO-PSO	Stage 1: GWO 40 it; Stage2: PSO 60 it, V_{max} = 0.70 (u-l)

Note: PSO = Particle Swarm Optimization, DE = Differential Evolution, GWO = Grey Wolf Optimizer, GA = Genetic Algorithm, HGWO-PSO = hybrid Grey Wolf Optimizer-Particle Swarm Optimization.

5.1 Wind profile scenario

Figure 7 illustrates the wind profile applied to the NREL 5 MW wind turbine during the simulation. The wind input is a deterministic composite signal generated in MATLAB. The profile was designed to provide a repeatable and representative operating scenario for evaluating the proposed pitch controller. The simulation was performed over 300 s using a fixed sampling interval of 0.02 s. A fixed random seed was used to generate the low-amplitude turbulence component, ensuring that the same wind realization can be reproduced in every simulation. The wind speed varies between 11.4 m/s and 25 m/s, allowing the turbine to operate around the Region II-III transition and throughout Region III. The composite wind profile consists of the following operating phases.

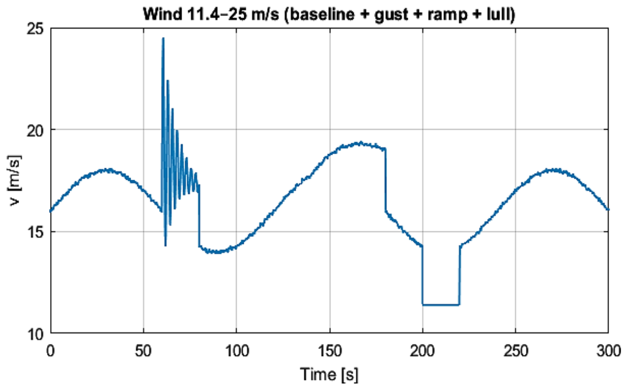

Figure 7. 4-Phase wind speed variation

0–60 s: A baseline turbulent wind with small fluctuations around ~17 m/s.

60–80 s: A strong gust event, characterized by a rapid and sharp increase in wind speed followed by high-frequency turbulence decay.

80–180 s: A smooth ramp-up and ramp-down section simulating gradual atmospheric variation.

180–230 s: A lull (drop in wind speed) down to approximately 12 m/s, representing a temporary reduction in available wind energy.

230–300 s: A mild sinusoidal fluctuation returning to moderate turbulence levels around 17–18 m/s.

These combined disturbances are used to stress-test the controller under realistic wind conditions encountered in utility-scale wind turbines. Such a composite profile ensures that controller performance is evaluated under gusts, transients, slow variations, and sudden lulls, enabling a fair and rigorous comparison of control strategies.

Table 3. Statistical characteristics of the generated wind profile over different operating intervals

Operation Interval	Time (s)	Mean Wind Speed (m/s)	Standard Deviation (m/s)	Turbulence Intensity (%)
Baseline	0-60	17.28	0.62	3.59
Gust	60-80	18.14	1.86	10.25
Ramp	80-180	16.80	2.02	12.02
Lull	180-230	13.50	1.76	13.04
Moderate turbulence	230-300	17.02	0.85	4.99
Overall	0-300	16.48	2.06	12.50

Table 3 summarizes the statistical characteristics of the generated wind profile for each operating interval. The baseline turbulence exhibits a turbulence intensity of 3.58%, whereas the overall variability increases because of the intentionally introduced gust, ramp, and lull events. These deterministic disturbances were included to evaluate the controller under representative operating conditions while ensuring full reproducibility of the simulations.

5.2 Speed regulation performance

5.2.1 Statistical evaluation

Table 4 summarizes the statistical performance of the conventional PSO and the proposed HGWO-PSO algorithm over five independent optimization runs. To ensure a fair comparison, both optimization methods used the same population size (40 individuals) and an identical computational budget of 30 optimization iterations. The standard PSO was executed for 30 iterations, while HGWO-PSO consisted of 10 iterations of GWO (global exploration) followed by 20 iterations of PSO (local exploitation). Despite converging to nearly identical PI controller gains, the proposed HGWO-PSO exhibited lower mean objective-function values together with reduced standard deviations, indicating better optimization repeatability and convergence robustness. The hybrid algorithm also achieved lower tracking-error indices (IAE and ITAE), slightly reduced overshoot, and noticeably lower cumulative pitch travel than the conventional PSO, demonstrating that the complementary exploration–exploitation mechanism improves controller tuning while preserving the same computational cost.

Table 5 summarizes the main control performance metrics for all optimization algorithms. The proposed hybrid GWO-PSO achieved the lowest IAE (132.7) and ITAE (13122.7), reflecting excellent speed tracking with minimal steady-state error. Additionally, the hybrid method maintained the lowest overshoot (14.71%), highlighting its superior transient response.

Table 4. Statistical comparison of Particle Swarm Optimization (PSO) and hybrid Grey Wolf Optimizer-Particle Swarm Optimization (HGWO-PSO) over five independent optimization runs

Performance Index	PSO (Mean ± Std)	PSO (Best)	HGWO-PSO (Mean ± Std)	HGWO-PSO (Best)
Objective function J	0.547 ± 0.011	0.539	0.541 ± 0.006	0.537
K_p	1.94 ± 0.04	1.95	1.94 ± 0.02	1.93
K_i	0.423 ± 0.06	0.422	0.422 ± 0.03	0.421
IAE	144.0 ± 3.5	142.6	133.8 ± 1.8	132.7
ITAE	13920 ± 210	13863	13280 ± 110	13122.7
Overshoot (%)	15.22 ± 0.25	15.19	14.76 ± 0.11	14.70
Control effect	171.2 ± 5.3	168.3	145.6 ± 2.6	142.6
RMS error	0.210 ± 0.010	0.203	0.194 ± 0.006	0.190
Steady-state error	0.041 ± 0.005	0.038	0.032 ± 0.003	0.030

Note: IAE = integral absolute error, ITAE = integral time-weighted absolute error, PSO = Particle Swarm Optimization, HGWO-PSO = hybrid Grey Wolf Optimizer-Particle Swarm Optimization.

Table 5. Performance comparison of meta-heuristic-tuned proportional-integral (PI) pitch controller

Method	IAE	ITAE	Over-Shoot (%)	Effort	[K_p, K_i]
Manual	173.9	16569.2	15.06	167.6	[2.57, 0.39]
PSO	142.6	13863.2	15.19	168.3	[1.95, 0.422]
GWO	133.9	13721.4	14.76	185.2	[1.95, 0.423]
DE	133.9	13721.3	14.77	185.0	[1.94, 0.424]
GA	133.8	13721.2	14.75	187.6	[1.97, 0.42]
HGWO -PSO	132.7	13122.7	14.71	142.6	[1.94 0.423]

Note: IAE = integral absolute error, ITAE = integral time-weighted absolute error, PSO = Particle Swarm Optimization, DE = Differential Evolution, GWO = Grey Wolf Optimizer, GA = Genetic Algorithm, HGWO-PSO = hybrid Grey Wolf Optimizer-Particle Swarm Optimization.

The hybrid strategy between the GWO and PSO consistently outperformed the standard algorithms, by achieving lower error indices and overshoot. The improvement is attributed to its balanced exploration–exploitation mechanism, which avoids premature convergence while refining gains during the later optimization stages.

5.3 Discussion

Figure 8 illustrates the evolution of the aerodynamic power coefficient (C_p) under the different optimization strategies. During periods of moderate wind speed, the turbine operates close to its maximum aerodynamic efficiency, resulting in relatively high C_p values. As the wind speed exceeds the rated value and the turbine enters Region III, the collective pitch controller progressively increases the blade pitch angle to regulate the generator speed. Consequently, the aerodynamic efficiency is intentionally reduced, leading to a decrease in C_p. This behavior is expected because, in Region III, the control objective shifts from maximizing energy capture to maintaining the rated generator speed while limiting aerodynamic loading. The proposed HGWO-PSO controller exhibits a smoother transition between the operating regions with reduced oscillations in C_p, indicating more stable pitch regulation under turbulent wind conditions. Overall, the results demonstrate that the controller achieves an appropriate balance between aerodynamic efficiency and speed regulation without introducing abrupt variations in the aerodynamic response.

Figure 9 shows the evolution of the tip-speed ratio λ (t) under the different control strategies throughout the varying wind conditions. At the beginning of the simulation, when the turbine operates near its optimal aerodynamic point, all controllers maintain λ around 5, which corresponds to efficient power extraction in region II. When the strong gust occurs (around 60–80 s), λ temporarily drops due to the sudden increase in aerodynamic torque. In this transient phase, the manually tuned PI and single-algorithm optimizers (PSO, DE, GWO, GA) exhibit noticeable oscillations, while the hybrid HGWO-PSO controller demonstrates a faster damping response and smaller fluctuation amplitude. During the gradual wind increase (80–180 s), λ decreases smoothly as the pitch controller transitions the turbine into region three (REG III), where speed regulation becomes dominant. Later, during the lull (180–300 s), λ rises again toward MPPT operation, and once more the hybrid controller shows the smoothest recovery, avoiding the overshoots observed in some other strategies.

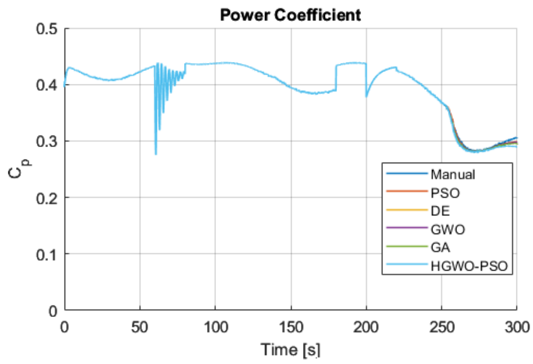

Figure 8. Evolution of power coefficient C_p over time

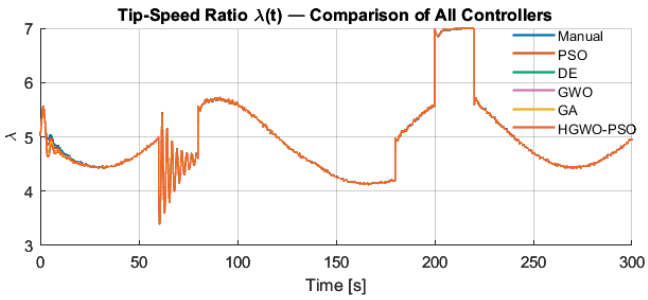

Figure 9. Tip-speed ratio λ evolution over time

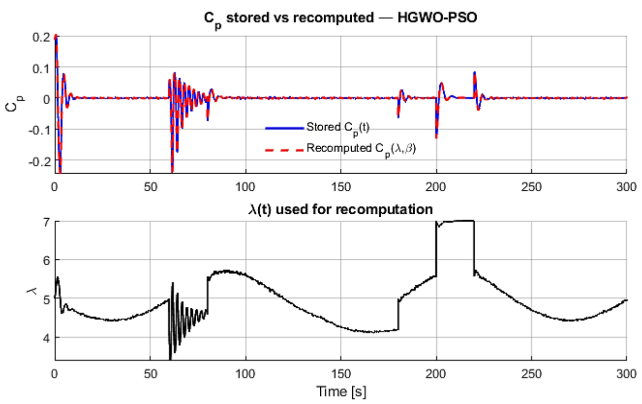

Figure 10. Internal consistency check of the aerodynamic power coefficient (C_p): comparison between the stored and recomputed values

Figure 10 presents an internal consistency check of the aerodynamic power coefficient computation. The solid blue curve represents the stored value of C_p (t) obtained during the simulation, while the dashed red curve corresponds to C_p recomputed afterward using the same aerodynamic equation C_p (λ, β). The close agreement between the two curves confirms the numerical consistency of the implementation, with only minor deviations observed during rapid transients due to numerical sensitivity. The lower subplot shows the corresponding evolution of the tip-speed ratio λ (t) used in the recomputation.

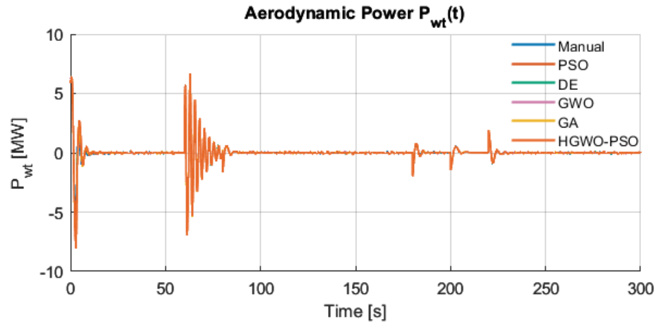

Figure 11. Aerodynamic power P_{wt} (t) (all algorithms)

Figure 11 shows the aerodynamic power P_{wt} extracted from the wind over time for each controller. During gust conditions, large fluctuations appear due to sudden changes in wind energy input. However, once the system settles into Region III operation, the aerodynamic power stabilizes around its rated value. The proposed HGWO-PSO strategy demonstrates a smoother recovery and reduced peak overshoots, indicating improved regulation of the blade pitch during strong disturbances. Some algorithms exhibit temporary power spikes or drops, reflecting less effective transient handling. Overall, the HGWO-PSO controller maintains a more stable aerodynamic power response under turbulent wind conditions, resulting in improved speed regulation and reduced actuator activity compared with the other optimization methods.

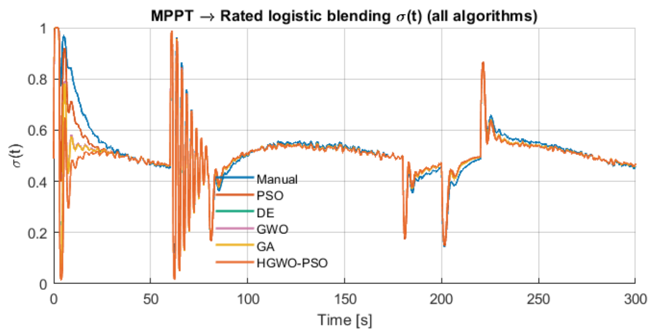

Figure 12. Logistic blending from Maximum Power Point Tracking (MPPT) to rated region

Figure 12 illustrates the evolution of the blending function σ (t), which provides a smooth transition between maximum power point tracking (MPPT, σ ≈ 1) and speed regulation in Region III (σ → 0). During the initial period and the wind-lull interval, σ (t) remains close to 1, indicating that the turbine prioritizes maximum energy capture. When the wind speed exceeds the rated value (approximately 60–80 s and again around 180–200 s), σ (t) rapidly decreases, allowing the controller to switch smoothly toward pitch-based speed regulation. Among the evaluated methods, the proposed HGWO-PSO controller exhibits smoother and better-damped transitions with fewer oscillations than the single meta-heuristic algorithms. This behavior indicates a more stable switching process between the operating regions under rapidly varying wind conditions, contributing to improved speed regulation and reduced control oscillations.

The generator and rotor speed responses (Figure 13) illustrate the ability of each control strategy to regulate the turbine operation under varying wind conditions. All controllers succeed in driving the system toward the rated generator speed of approximately 123 rad/s; however, the HGWO-PSO controller achieves the fastest settling and lowest oscillations following disturbances, while the manually tuned controller shows visibly slower damping and longer transient oscillation levels. During transient gusts (around 60–80 s) and deep wind dips (around 180–230 s), the hybrid controller demonstrates superior disturbance rejection, maintaining smooth and tightly regulated speed trajectories. In contrast, standard meta-heuristic approaches exhibit slightly larger recovery. Overall, the hybrid strategy provides the best balance between speed stability and dynamic responsiveness.

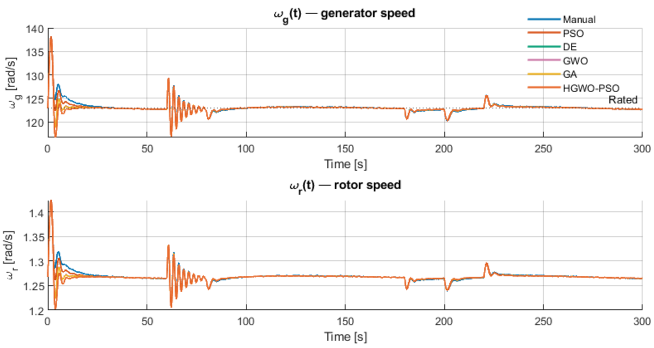

Figure 13. Rotor and generator speed variation

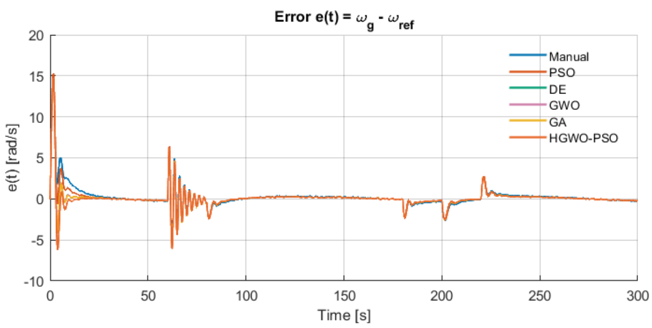

Figure 14. Error speed variation

The tracking error plots (Figure 14) confirm the effectiveness of the hybrid optimization in reducing steady-state and transient error. The HGWO-PSO controller rapidly drives the error to near zero, exhibiting minimal overshoot and no prolonged oscillations. During gust and lull periods, the hybrid controller maintains the smallest magnitude of deviation, demonstrating strong robustness against aerodynamic disturbances. PSO, DE, GWO, and GA also converge to acceptable performance, but they present slightly higher error peaks, suggesting slower corrective action. The manually tuned controller shows the largest tracking error, confirming that heuristic or manual parameter adjustment is insufficient for highly dynamic wind conditions. These results validate that the hybrid method provides enhanced precision in speed tracking.

Figure 15 shows the pitch angle trajectories under the different control strategies. The pitch commands generated by the proposed HGWO-PSO controller are smoother and exhibit fewer abrupt changes than those produced by the other controllers. This behavior indicates reduced cumulative pitch travel and smoother actuator operation. In contrast, the manually tuned controller tends to react more slowly to wind disturbances. Overall, the proposed HGWO-PSO controller achieves stable pitch regulation while reducing unnecessary pitch activity under varying wind conditions.

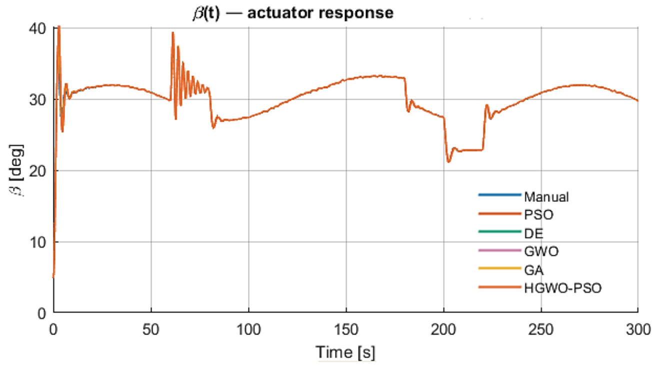

Figure 15. Pitch angle evaluation for all meta-heuristic algorithms

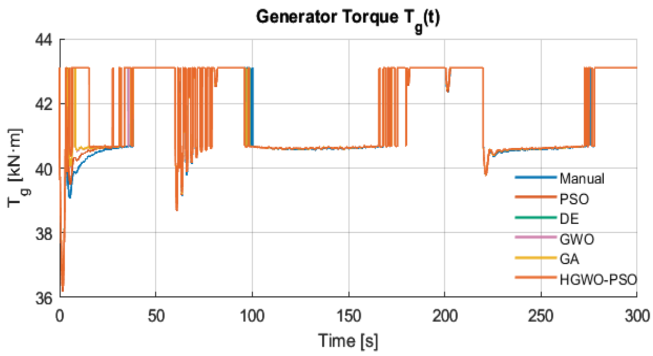

Figure 16. Generator torque variation

Figure 16 shows the generator torque response under the different control strategies. All controllers ultimately regulate the generator torque around its rated value (approximately 43 KN·m). However, the proposed HGWO-PSO controller provides a smoother torque transition, particularly during rapid wind disturbances. The torque responses obtained with the single meta-heuristic algorithms exhibit more noticeable transient oscillations, whereas the manually tuned PI controller shows slower recovery following wind variations. Overall, the HGWO-PSO controller provides smoother torque regulation and improved transient performance, demonstrating its effectiveness for speed regulation under variable wind conditions.

Figure 17 illustrates the evolution of the proportional (K_p) and integral (K_i) gains during the optimization process for the different tuning algorithms. During the initial iterations, PSO, DE, GWO, and GA exhibit noticeable fluctuations in both controller gains, reflecting the exploration phase of the optimization process. Among the single meta-heuristic algorithms, GWO and GA show relatively larger oscillations before gradually approaching stable gain values. As the optimization progresses, all algorithms converge to nearly identical K_p and K_i values, indicating convergence to the same near-optimal region of the search space. The proposed HGWO-PSO algorithm reaches this region with a smoother convergence trajectory and reduced gain oscillations during the optimization process. This behavior reflects a more effective balance between the global exploration capability of GWO and the local exploitation capability of PSO, leading to improved convergence stability and repeatability. The convergence characteristics observed in Figure 17 are consistent with the dynamic performance presented in the previous figures. The final controller gains are similar for all optimization methods. The smoother convergence obtained with HGWO-PSO contributes to lower tracking errors, reduced overshoot, and decreased cumulative pitch activity, thereby providing a more robust and reliable PI controller tuning under variable wind conditions.

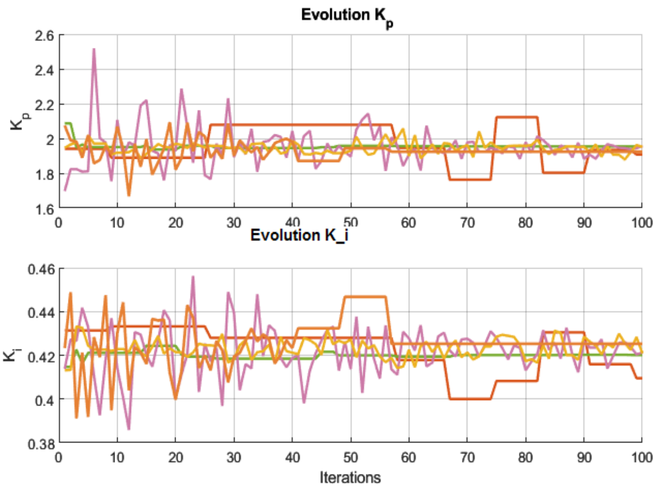

Figure 17. Evolution of proportional-integral (PI) gains during optimization for all meta-heuristic algorithms

Figure 18 provides a comparative illustration of the controller performances based on four key metrics: IAE, ITAE, overshoot, and actuator effort. The Hybrid GWO-PSO controller encloses the smallest area on the radar plot. This indicates: Lower IAE and ITAE (faster and more accurate tracking of rated generator speed). Reduced actuator effort (smoother pitch motion and potentially longer actuator life). Controlled overshoot (dynamic stability maintained even during gust events).

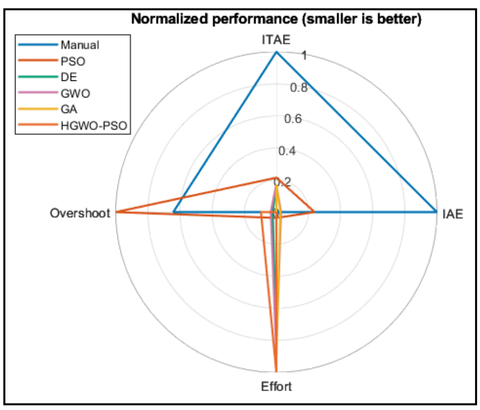

Figure 18. Multi-criteria performance evaluation of proportional-integral (PI) pitch controllers (radar comparison)

The bar chart in Figure 19 compares the performance of all controllers in terms of IAE, ITAE, overshoot, and cumulative pitch travel. The proposed HGWO-PSO controller achieves the lowest IAE and ITAE values, indicating better tracking accuracy. It also reduces overshoot and cumulative pitch travel compared with the other optimization methods, showing smoother pitch control actions under variable wind conditions.

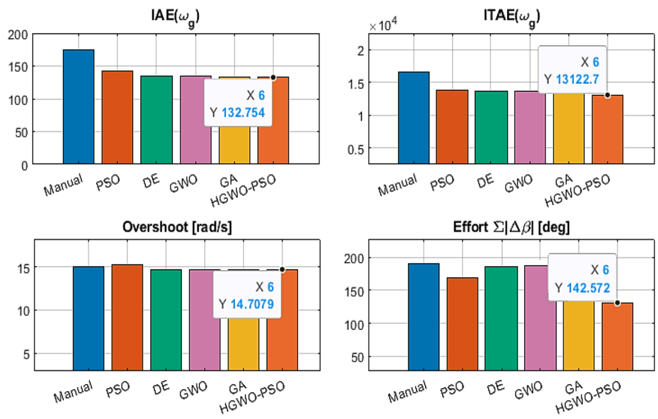

Figure 19. Performance comparison of proportional-integral (PI) pitch controller across all optimization algorithms

6. CONCLUSIONS

This paper presented a high-fidelity nonlinear model and a comparative study of PI pitch controller tuning for a 5 MW utility-scale wind turbine equipped with a two-mass drive-train using different meta-heuristic optimization algorithms. Simulations under variable wind conditions (11.4–25 m/s) demonstrated that the proposed HGWO-PSO controller consistently achieved improved overall performance compared with the standalone PSO, GWO, DE, and GA algorithms. Specifically, the hybrid approach obtained lower integral error indices (IAE and ITAE), minimized overshoot, and reduced cumulative pitch travel. Moreover, the responses of the power coefficient (Cp), tip-speed ratio (λ), and generator torque demonstrated stable controller behavior during the transition between Region II and Region III and under above-rated wind conditions. The results also demonstrate the importance of using a high-fidelity wind turbine model that includes nonlinear aerodynamics, a two-mass drivetrain, and pitch actuator constraints to obtain a realistic evaluation of controller performance. The benchmarking protocol adopted in this work, involving identical wind profiles, optimization settings, population sizes, iteration counts, and objective functions for all algorithms, ensured fair and reproducible comparison. The proposed HGWO-PSO algorithm represents an effective optimization approach for PI pitch controller tuning in large wind turbines operating under variable wind conditions.

REFERENCES

[1] Chien, F.S., Kamran, H.W., Albashar, G., Iqbal, W. (2021). Dynamic planning, conversion, and management strategy of different renewable energy sources: A sustainable solution for severe energy crises in emerging economies. International Journal of Hydrogen Energy, 46(11): 7745-7758. https://doi.org/10.1016/j.ijhydene.2020.12.004

[2] Gayen, D., Chatterjee, R., Roy, S. (2024). A review on environmental impacts of renewable energy for sustainable development. International Journal of Environmental Science and Technology, 21(5): 5285-

5310. https://doi.org/10.1007/s13762-023-05380-z

[3] Jayachandran, M., Gatla, R.K., Rao, K.P., Rao, G.S., Mohammed, S., Milyani, A.H., Azhari, A.A., Kalaiarasy, C., Geetha, S. (2022). Challenges in achieving Sustainable Development Goal 7: Affordable and clean energy in light of nascent technologies. Sustainable Energy Technologies and Assessments, 53: 102692. https://doi.org/10.1016/j.seta.2022.102692

[4] Papadis, E., Tsatsaronis, G. (2020). Challenges in the decarbonization of the energy sector. Energy, 205: 118025. https://doi.org/10.1016/j.energy.2020.118025

[5] Giedraityte, A., Rimkevicius, S., Marciukaitis, M., Radziukynas, V., Bakas, R. (2025). Hybrid renewable energy systems—A review of optimization approaches and future challenges. Applied Sciences, 15(4): 1744. https://doi.org/10.3390/app15041744

[6] Jonkman, J.M., Butterfield, S., Musial, W., Scott, G. (2009). Definition of a 5-MW reference wind turbine for offshore system development. National Renewable Energy Laboratory. https://doi.org/10.2172/947422

[7] Rezaei, A., Guo, Y., Keller, J., Nejad, A.R. (2023). Effects of wind field characteristics on pitch bearing reliability: A case study of 5 MW reference wind turbine at onshore and offshore sites. Forschung im Ingenieurwesen, 87(1): 321-338. https://doi.org/10.1007/s10010-023-00654-x

[8] Hummel, J.I., Kober, J., Mulders, S.P. (2025). Output-constrained individual pitch control methods using the multiblade coordinate transformation: Trading off actuation effort and blade fatigue load reduction for wind turbines. Wind Energy Science, 10(9): 2005-2023. https://doi.org/10.5194/wes-10-2005-2025

[9] Gambier, A. (2024). Actuators for large wind energy systems—A tutorial-focused survey. Actuators, 13(10): 416. https://doi.org/10.3390/act13100416

[10] Rajendran, S., Jena, D. (2014). Control of variable speed variable pitch wind turbine at above and below rated wind speed. Journal of Wind Energy, 2014(1): 709128. https://doi.org/10.1155/2014/709128

[11] Lubosny, Z., Bialek, J.W. (2007). Supervisory control of a wind farm. IEEE Transactions on Power Systems, 22(3): 985-994. https://doi.org/10.1109/TPWRS.2007.901101

[12] Abdelbaky, M.A., Liu, X., Jiang, D. (2020). Design and implementation of partial offline fuzzy model-predictive pitch controller for large-scale wind-turbines. Renewable Energy, 145: 981-996. https://doi.org/10.1016/j.renene.2019.05.074

[13] Navarrete, E.C., Perea, M.T., Correa, J.J., Serrano, R.C., Moreno, G.R. (2019). Expert control systems implemented in a pitch control of wind turbine: A review. IEEE Access, 7: 13241-13259. https://doi.org/10.1109/ACCESS.2019.2892728

[14] Hassan, A., Ahmad, G., Shafiullah, M., Islam, A., Alam, M.S. (2025). Review of the intelligent frameworks for pitch angle control in wind turbines. IEEE Access, 13: 29864-29885. https://doi.org/10.1109/ACCESS.2025.3540367

[15] Jaber, A.S., Mahdi, H.B., Abdul-jabbar, T.A., et al. (2024). A comprehensive overview of wind turbine controller technology: Emerging trends and challenges. Wind Engineering, 48(5): 954-975. https://doi.org/10.1177/0309524X241230632

[16] Kennedy, J., Eberhart, R. (1995). Particle swarm optimization. In Proceedings of ICNN'95-International Conference on Neural Networks, Perth, WA, Australia, pp. 1942-1948. https://doi.org/10.1109/ICNN.1995.488968

[17] Mirjalili, S., Mirjalili, S.M., Lewis, A. (2014). Grey wolf optimizer. Advances in Engineering Software, 69: 46-61. https://doi.org/10.1016/j.advengsoft.2013.12.007

[18] Goldberg, D.E. (1989). Genetic algorithms in search, optimization, and machine learning. Addison.

[19] Storn, R., Price, K. (1997). Differential evolution–A simple and efficient heuristic for global optimization over continuous spaces. Journal of Global Optimization, 11(4): 341-359. https://doi.org/10.1023/A:1008202821328

[20] Poultangari, I., Shahnazi, R., Sheikhan, M. (2012). RBF neural network based PI pitch controller for a class of 5-MW wind turbines using particle swarm optimization algorithm. ISA Transactions, 51(5): 641-648. https://doi.org/10.1016/j.isatra.06.2012.001

[21] Benamara, K., Amimeur, H., Hamoudi, Y., Abdolrasol, M.G., Cali, U., Ustun, T.S. (2024). Grey wolf optimization for enhanced performance in wind power system with dual-star induction generators. Frontiers in Energy Research, 12: 1421336. https://doi.org/10.3389/fenrg.2024.1421336

[22] Shaikh, M.S., Lin, H., Xie, S., Dong, X., Lin, Y., Shiva, C.K., Mbasso, W.F. (2025). An intelligent hybrid grey wolf-particle swarm optimizer for optimization in complex engineering design problem. Scientific Reports, 15(1): 18313. https://doi.org/10.1038/s41598-025-02154-0

[23] Nguyen, T.L., Nguyen, Q.A. (2025). A multi-objective PSO-GWO approach for smart grid reconfiguration with renewable energy and electric vehicles. Energies, 18(8): 2020. https://doi.org/10.3390/en18082020

[24] Ebraheem, M., Jyothsna, T.R. (2024). Hybrid sand cat-galactic swarm optimization-based adaptive maximum power point tracking and blade pitch controller for wind energy conversion system. International Journal of Adaptive Control and Signal Processing, 38(11): 3575-3597. https://doi.org/10.1002/acs.3890

[25] Gambier, A. (2021). Pitch control of three bladed large wind energy converters—A review. Energies, 14(23): 8083. https://doi.org/10.3390/en14238083

[26] Song, Y., Jeon, T., Paek, I., Dugarjav, B. (2022). Design and validation of pitch H-infinity controller for a large wind turbine. Energies, 15(22): 8763. https://doi.org/10.3390/en15228763

[27] Menezes, E.J., Araújo, A.M. (2023). Wind turbine structural control using H-infinity methods. Engineering Structures, 286: 116095. https://doi.org/10.1016/j.engstruct.2023.116095

[28] Owen, E., Pieper, J. (2021). The augmented unscented H-infinity transform with H-infinity filtering for effective wind speed estimation in wind turbines. In 2021 IEEE Electrical Power and Energy Conference (EPEC), Toronto, ON, Canada, pp. 163-170. https://doi.org/10.1109/EPEC52095.2021.9621396

[29] Arturo Soriano, L., Yu, W., Rubio, J.D.J. (2013). Modeling and control of wind turbine. Mathematical Problems in Engineering, 2013(1): 982597. https://doi.org/10.1155/2013/982597

[30] Arabi, M., Zennir, Y., Bounezour, H., Benghanem, M., Garcia, J.E.S., Wadi, M. (2025). Novel nonlinear PI

controller using meta-heuristic algorithms for speed control of wind turbine systems. Journal Européen des Systèmes Automatisés, 58(8): 1593-1608. https://doi.org/10.18280/jesa.580805

[31] Dari, H., Mehenaoui, L., Ramdani, M. (2015). An optimized fuzzy controller to capture optimal power from wind turbine. In 2015 International Conference on Renewable Energy Research and Applications (ICRERA), Palermo, Italy, pp. 815-820. https://doi.org/10.1109/ICRERA.2015.7418525

[32] Kamel, R.M., Chaouachi, A., Nagasaka, K. (2011). Enhancement of micro-grid performance during islanding mode using storage batteries and new fuzzy logic pitch angle controller. Energy Conversion and Management, 52(5): 2204-2216. https://doi.org/10.1016/j.enconman.2010.12.025

[33] Salih, B.M., Hamoodi, S.A., Hamoodi, A.N. (2024). Enhancing the behavior of small scale wind turbine based on fuzzy logic system. Journal Européen des Systèmes Automatisés, 57(1): 147-153. https://doi.org/10.18280/jesa.570115

[34] Munteanu, I., Cutululis, N.A., Bratcu, A.I., Ceangă, E. (2008). Optimal Control of Wind Energy Systems: Towards a Global Approach. Springer London. https://doi.org/10.1007/978-1-84800-080-3

[35] Badjıe, A.K., Kalyon, M. (2019). Nonlinear control of power coefficients in wind turbines. İstanbul Ticaret Üniversitesi Teknoloji ve Uygulamalı Bilimler Dergisi, 1(2): 1-15. https://dergipark.org.tr/tr/pub/icujtas/article/806483.

[36] Boukhezzar, B., Siguerdidjane, H. (2005). Nonlinear control of variable speed wind turbines without wind speed measurement. In Proceedings of the 44th IEEE Conference on Decision and Control, Seville, Spain, pp. 3456-3461. https://doi.org/10.1109/CDC.2005.1582697

[37] Asgharnia, A., Shahnazi, R., Jamali, A. (2018). Performance and robustness of optimal fractional fuzzy PID controllers for pitch control of a wind turbine using chaotic optimization algorithms. ISA Transactions, 79: 27-44. https://doi.org/10.1016/j.isatra.2018.04.016

[38] Karami-Mollaee, A., Barambones, O. (2022). Pitch control of wind turbine blades using fractional particle swarm optimization. Axioms, 12(1): 25. https://doi.org/10.3390/axioms12010025

[39] Dari, H., Mehenaoui, L., Ramdani, M. (2015). Fuzzy gain scheduled output feedback control for variable-speed variable-pitch wind turbine. In International Conference on Automatic Control, Telecommunications and Signals (ICATS15), Annaba, Algeria, pp. 1-6. https://www.researchgate.net/publication/326677795.

[40] Boukhezzar, B., Siguerdidjane, H. (2010). Nonlinear control of a variable-speed wind turbine using a two-mass model. IEEE Transactions on Energy Conversion, 26(1): 149-162. https://doi.org/10.1109/TEC.2010.2090155

[41] Hwas, A., Katebi, R. (2012). Wind turbine control using PI pitch angle controller. IFAC Proceedings Volumes, 45(3): 241-246. https://doi.org/10.3182/20120328-3-IT-3014.00041

[42] Azlan, F., Kurnia, J.C., Tan, B.T., Ismadi, M.Z. (2021). Review on optimisation methods of wind farm array under three classical wind condition problems. Renewable and Sustainable Energy Reviews, 135: 110047. https://doi.org/10.1016/j.rser.2020.110047

[43] Menezes, E.J.N., Araújo, A.M., Da Silva, N.S.B. (2018). A review on wind turbine control and its associated methods. Journal of Cleaner Production, 174: 945-953. https://doi.org/10.1016/j.jclepro.2017.10.297

[44] Samani, A.E., De Kooning, J.D., Kayedpour, N., Singh, N., Vandevelde, L. (2020). The impact of pitch-to-stall and pitch-to-feather control on the structural loads and the pitch mechanism of a wind turbine. Energies, 13(17): 4503. https://doi.org/10.3390/en13174503

[45] Njiri, J.G., Söffker, D. (2016). State-of-the-art in wind turbine control: Trends and challenges. Renewable and Sustainable Energy Reviews, 60: 377-393. https://doi.org/10.1016/j.rser.2016.01.110

[46] Serrano-Balbontín, A.J., Blas, I.T., Vinagre, M. (2024). Neuron-based back-calculation anti-windup strategy: first results. IFAC-PapersOnLine, 58(7): 388-393. https://doi.org/10.1016/j.ifacol.2024.08.093

[47] Jiao, X., Wang, G., Wang, X., Zhang, Z., Tian, Y., Fan, X. (2024). Anti-windup pitch angle control for wind turbines based on bounded uncertainty and disturbance estimator. Journal of Marine Science and Engineering, 12(3): 473. https://doi.org/10.3390/jmse12030473

[48] Noureddine, S., Morsli, S., Tayeb, A., Mouloud, D. (2021). Optimal fractional-order pi control design for a variable speed PMSG-based wind turbine. Journal Européen des Systèmes Automatisés, 54(6): 915-922. https://doi.org/10.18280/jesa.540615

[49] Amrane, A., Zennir, Y. (2024). Performance analysis of nature-inspired algorithms for PID control of electric wheelchairs. International Journal of Automation and Safety, 2(2): 14-19. https://asjp.cerist.dz/en/article/260884.